Maximizing Robotic Limb Rigidity and Strain Sensing Capabilities Through Localized Kevlar Fiber Reinforcement

Gesa F. Dinges[1], Isabella Kudyba[1], Sasha N. Zill[2], and Nicholas S. Szczecinski[1(✉)]

[1] Neuro-Mechanical Intelligence Laboratory, Department of Mechanical, Materials and Aerospace Engineering, West Virginia University, Morgantown, WV 26506, USA
imk00001@mix.wvu.edu, nicholas.szczecinski@mail.wvu.edu

[2] Department of Anatomy and Pathology, Joan C. Edwards School of Medicine, Marshall University, Huntington, WV 25704, USA

Abstract. Strain can provide important sensory information for locomotor control in both robots and insects. Strain measurements in limbs can indicate forces that resist movements generated by actuators or muscle. Key time points in stepping can be monitored through changes in strain and inform the neuromuscular or robotic control system of the step cycle phase, allowing for modifications during unplanned events. For both systems, there is a trade-off between the limb rigidity and thus accuracy of limb positioning, and the magnitude (i.e., sensitivity) of strain measurements. Rigid limb segments enable precise end effector (e.g., foot) placement but reduce the strain magnitude when force is resisted; compliant limb segments increase the strain magnitude, but extreme compliance can potentially decrease precision in determination of limb position and movement. Robotic limb segments typically have homogeneous material properties, requiring the choice between rigidity and compliance. In contrast, insect limbs have spatial gradients of material properties. We show the benefits of localized Kevlar fiber reinforcement for strain sensing in robotic limb segments. While full-segment Kevlar reinforcement solely increases rigidity, the most effective reinforcement format for increasing both rigidity and strain magnitude is partial fiber supplementation encompassing the majority of the limb segment but not the area where strain is monitored. We propose that future robotic additive manufacturing should incorporate material heterogeneity to optimize rigidity and strain sensing capabilities.

Keywords: 3D-printing · Kevlar · heterogeneous materials · legged locomotion

1 Introduction

Traversing rugged terrain using legs benefits from the measurement of forces acting on the limbs. Animals make use of force information in the control of walking by monitoring the strain of compliant body parts in series between the actuator and the

G. F. Dinges, I. Kudyba and S.N. Zill—These authors contributed equally to this work.

N. S. Szczecinski et al. (Eds.): Living Machines 2024, LNAI 14930, pp. 83–93, 2025.
https://doi.org/10.1007/978-3-031-72597-5_6

point of force application. Vertebrates monitor tendon strain using Golgi tendon organs [1] and insects monitor exoskeletal strain using campaniform sensilla (CS) [2, 3]. The nervous systems of these animals use this sensory feedback to adapt motor output in a context-appropriate manner [4]. To produce robots whose motions are as agile and adaptable as those of animals, we seek to incorporate this type of force feedback into their control systems.

In insects, campaniform sensilla, which detect deformations of the exoskeleton that occur when contractions of leg muscles are resisted, monitor strain. Information from the sensilla is used to adapt muscle forces in posture and locomotion. In walking robots, force can be monitored using load cells or strain gauges [5–7]. Load cells are extremely rigid and linearly encode strain, which requires high signal amplification and, consequently, makes them susceptible to noise. Strain gauges applied to polymer robot parts, on the other hand, allow high-resolution encoding of directional strain and have been utilized in walking robots [5–7]. While classic strain gauge rosettes are beneficial in locomoting robots, the development of novel strain gauge techniques, such as strain gauges developed using gradient stiffness sliding [8] and stretchable pressure sensors [9] may prove to be beneficial in future application due to their high sensitivity.

Both insect and robotic force measurement systems are affected by their material make-up and its effects on strain propagation (e.g., during contact with the ground). Furthermore, for both systems to have the most predictable kinematics possible, maximally stiff limbs are most beneficial. The exoskeleton of adult insects is stiff due to both the presence of rigid chitin fibers and the crosslinking and sclerotization of the protein matrix in which the fibers are embedded. In robot manipulators, kinematics and dynamics assume that the bodies that make up the arm are rigid [10]. However, the material stiffness of both cuticle and robotic parts has the potential to decrease strain signals, making the utilization of this important sensory information difficult. In insects, stiffness is elegantly incorporated with strain sensing capabilities through the heterogeneous material properties of the cuticle [11, 12]. For example, in some insects the exoskeleton is thin at the locations of the campaniform sensilla [13, 14]. However, the chitin fibers in the cuticle surrounding the receptor caps are concentrated and oriented to distribute the effects of stresses around the sense organ [15]. This ensures that each sensillum has exquisite sensitivity in detecting strain while maintaining high stiffness in the surrounding leg cuticle. For robust robotic control, similar stiffness maximization while ensuring strain measurability could also be beneficial.

In line with advancements in 3D-printing techniques for robotic parts, altering the fiber ratios in robotic limb segments may improve strain sensing capabilities while maintaining limb stiffness for kinematic control. Kevlar fiber reinforcement has a higher impact resistance than carbon fiber [16]. To investigate how this reinforcement may benefit distributed sensing in walking robots, we analyzed strain sensing in dynamically scaled robotic models of insect tibias. We used three different tibias, each with different proportions of Kevlar reinforcement. We displaced the distal end of each tibia transversal to the tibia's long axis (i.e., as a cantilever beam) and measured the restoring force applied by the tibia and the strain at a proximal site at a similar location to where CS would be located in the insect.

Our results clearly showed that partial Kevlar reinforcement of the tibia distal to the strain gauge site is the beneficial solution for maintaining tibial rigidity while increasing the magnitude of strain at the sensor location. The strains monitored in a partially fiber reinforced limb segment (i.e., distal to the strain gauge) were greater than those monitored in a non-reinforced limb segment. However, the signal to noise ratio was not improved through fiber supplementation compared to no fiber reinforcement. Consequently, fiber supplementation increases rigidity but not the signal to noise ratio. The partially reinforced segment was more rigid than no fiber reinforcement. The fully reinforced limb segment showed significantly reduced strain signals compared to partial and no fiber reinforcement and its surface was always in tension, never in compression. Based on these results, we propose the consideration of partial Kevlar reinforcement in additively manufactured components in future walking robots to enhance force sensing.

2 Material and Methods

We utilized a dynamically scaled, biomimetic stick insect leg segment for all experiments. The robotic limb used for these experiments was first published in Zyhowski et al., 2022. Each leg segment sample was a hollow square tube, which modeled the hollow exoskeleton of an arthropod while remaining easy to manufacture. Most Markforged 3D-printers have the capability to add reinforcement fibers to increase the part's strength while simultaneously printing the part out of plastic. Using Eiger software (Markforged Inc., Waltham, MA, USA), we 3D-printed (Mark 2; Markforged Inc.) limb segments out of Onyx® ([17]; Markforged Inc.) with and without Aramid Fiber (*Kevlar* [16]; Markforged Inc.) reinforcement. We created three versions of the tibial leg segment (n = 1) with varying amounts of fiber reinforcement. As this is a preliminary study and due to the high cost of strain gauges each model was tested once. The first model had no Kevlar fiber reinforcement (*no-fiber model*, Fig. 1A). The second model had Kevlar fiber throughout the complete shaft (*full-fiber model*; 118.5 mm of Kevlar, Fig. 1A). The third model was printed with Kevlar fiber throughout the shaft from the distal end up to 20 mm from the proximal end (*partial-fiber model*, 98.5 mm of Kevlar, Fig. 1A). Reinforcement fibers are added and controlled in the Eiger software under the "XRAY" tab. All layers of the part were selected. The Kevlar fibers were printed with an isotropic solid fill and fibers were aligned with the axial direction of the leg segment (Fig. 1B). In the *partial-fiber* model, the region of reinforcement fiber is selected in the software by selecting the distal end of the leg segment to a small bump in the design that is later sanded off.

On all legs, we manually glued strain gauge rosettes (Micro-Measurements C5K-06-S5198–350-33F; Vishay Intertechnology, Malvern, PA, USA; Grid resistance, 350.0 Ω ± 0.5%) on the dorsal side, 10 mm distal to the proximal end of the shaft (Fig. 1A). They were aligned along the transverse and axial axes of the segment. In order to compare strain measurements between models, we aligned the strain gauges and tibia using a 3D-printed guide. The strain gauge signals were amplified using operational amplifiers (Texas Instruments, Dallas, Tx., USA; IC OPAMP GP 4 CIRCUIT 14SOIC) and converted to 12-bit digital signals using a microcontroller OpenCM 9.04 Board (Robotis Inc., Lake Forest, CA, USA).

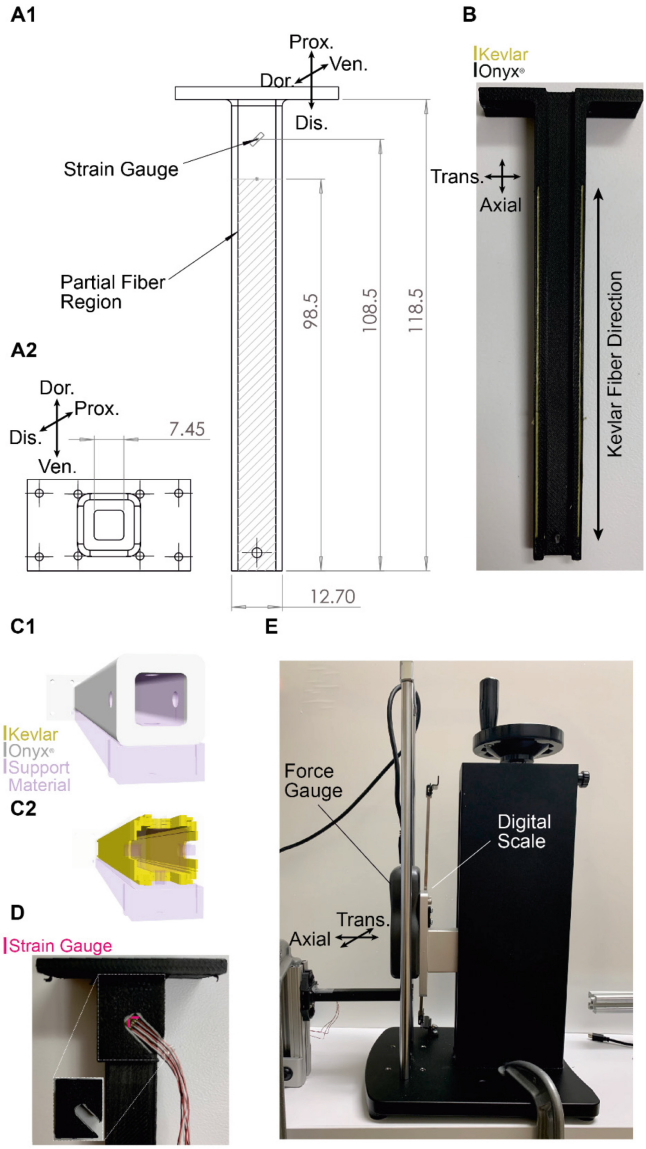

Fig. 1. Models and setup design; **A1** schematic of the robotic tibia leg segment; the shaft was printed in three different manners: 1) the full 118.5 mm were printed using Onyx® only (*no-fiber* model); 2) the full 118.5 mm were printed using Onyx® and Kevlar reinforcement (*full-fiber* model); 3) the distal most 98.5 mm were printed using Onyx® and Kevlar reinforcement (area marked with hatch marks), while the remaining 20 mm were printed using Onyx® only (*partial-fiber* model). The strain gauges were placed 10 mm from the proximal shaft end, with an axial and transverse axis orientation. Prox.: proximal, Dis.: distal, Dor.: dorsal, Ven.: ventral; **A2** front view of the model's proximal end; **B** partially printed *partial-fiber* model; yellow fibers are Kevlar; **C1** model as seen in Eiger software, without Kevlar; **C2** model as seen in Eiger software, with Kevlar; **D** proximal end of tibia with strain gauge guide and attached stain gauge rosette; magenta lines mark the axes of the strain gauge rosette; insert shows strain gauge guide; **E** image of the general setup; each model's distal end is aligned with the force probe.

To test the effects of Kevlar on strain measurements and limb displacement during loading, we utilized a manual hand wheel-operated test stand (FGS-250W; Nidec-Shimpo, Kyoto, Japan). The force was monitored with a digital force gauge (1000 N ± 0.3% full scale accuracy; FG-3009; Nidec-Shimpo). The hand wheel included a tensile frame kit (FGS-250W-TFK; Nidec-Shimpo) to monitor displacement. Each model was attached to a slotted t-rail at its proximal end using a 3D-printed bracket (Fig. 1A). The distal end was aligned with the force probe (Fig. 1B, C). We displaced the distal end of each model in 0.05–0.10 mm increments to a maximum displacement of 4.5 mm. At this peak displacement, the models underwent a constant displacement test for 180 s. Following this phase, the displacement was reduced back to the starting value of 0 mm. The mechanical displacement was performed manually while displacement values, force, and strain were monitored using MATLAB (2021b; MathWorks, Natick, MA, USA).

We performed a least-squares fit of the hysteresis of the force probe measurement over time with a Generalized Maxwell model [18], which predicts force relaxation as an exponential decay,

$$F = a_1 \cdot \exp(b_1 \cdot t) + c_1, \tag{1}$$

where a is the magnitude of the stress relaxation, b describes the time course of stress relaxation, and c is the force at which stress relaxation ends. This model was chosen because of the observed decay profile of the force probe measurement over time. The time constant of hysteresis is $\tau = -1/b$. To correct the fit in the *no-fiber* model that had low force changes over time, we prolonged the hold phase to 360 s and used this data exclusively for curve fitting.

To analyze the signal-to-noise ratio (SNR) of the strain measurements, we performed a least-squares fit of the strain data over time with an exponential curve similarly to force using the Generalized Maxwell model,

$$\varepsilon = a_2 \cdot \exp(b_2 \cdot t). \tag{2}$$

The noise was calculated by comparing the data with the least-squares fit, then the SNR was calculated by dividing the power of the fit over the power of the noise.

3 Results

All models showed changes in monitored strain during displacement (Fig. 2A). All three models showed axial elongation during displacement, while transverse compression was only observed in the *no-fiber* and *partial-fiber* models. In contrast, the transverse axis of the *full-fiber* model elongated during displacement. Along both the axial and transverse axes, the *partial-fiber* model had the greatest strain gauge measurements. The lowest overall strain was monitored in the *full-fiber* model.

There was a clear correlation between Kevlar reinforcement and monitored force during displacement (i.e., segment rigidity; Fig. 2B). The greatest force was monitored in the *full-fiber* model, while the lowest force was monitored in the *no-fiber* model. The peak measured force (at 4.5 mm of transverse, distal deflection) was 32 N in the *full-fiber* model, 22 N in the *partial-fiber* model, and 11 N in the *no-fiber* model.

The strain measurements during displacement showed clear hysteresis loops, and thus energy dissipation, between loading and unloading (Fig. 3A1–2). The greatest difference between strain measurements during loading and unloading was seen within both the transverse and axial axes of the *partial-fiber* model. The least change in strain was seen in the *full-fiber* model. All models had greater strain gauge magnitudes during load application (Fig. 3A1–A2).

During the constant displacement test at peak displacement, all three models showed stress relaxation (Fig. 3B1–3). The *no-fiber* model had a force relaxation of 9.2%; the *full-fiber* model of 13.5%; and the *partial-fiber* model of 12.5%. The fastest force decay was present in the *no-fiber* model followed by the *full-fiber* model and the *partial-fiber* model (Table 1 [*b*]). The force magnitude decreased most in the *full-fiber* model followed by the *partial-fiber* model and the *no-fiber* model (Table 1 [*a*]).

Table 1. Fit coefficient results [Eq. 1].

	No-Fiber Model	Full-Fiber Model	Partial Fiber Model
a_1	2.055	4.263	2.778
b_1	−0.009708	−0.01133	−0.01186
c_1	8.892	27.33	19.53
$a_1/(a_1 + c_1)$	0.188	0.135	0.125
τ	103 s	88.3 s	84.3 s

The SNR in the *no-fiber* model was 48.5 dB along the axial axis and 44.7 dB along the transverse axis. In the *full-fiber* model, the SNR was 26.3 dB along the axial axis and 29.3 dB along the transverse axis. In the *partial-fiber* model, the SNR along was 42.5 dB the axial axis and 44.1 dB along the transverse axis.

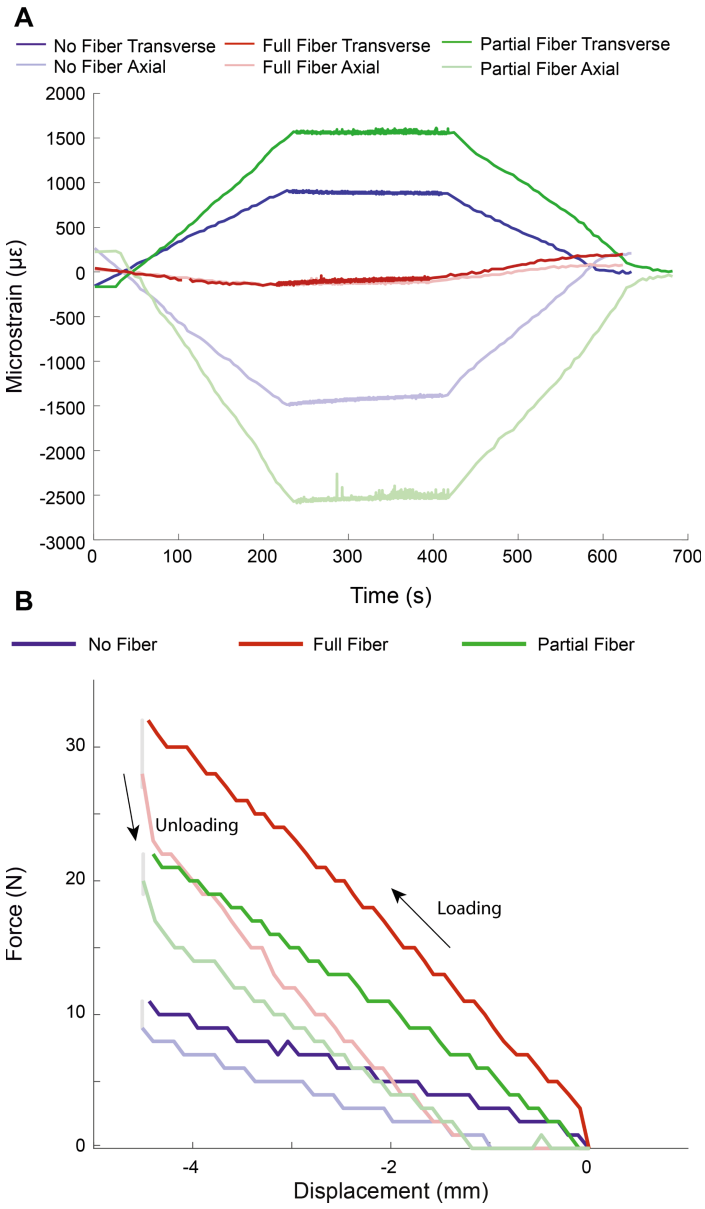

Fig. 2. Microstrain and force measurements of each limb segment during displacement; **A** microstrain measurements along the axial and transverse axis of the three different models during a 4.5 mm displacement of the distal end (positive values represent compression); **B** monitored force at the distal end of each model during displacement. Gray lines represent the decrease in force during the constant displacement phase.

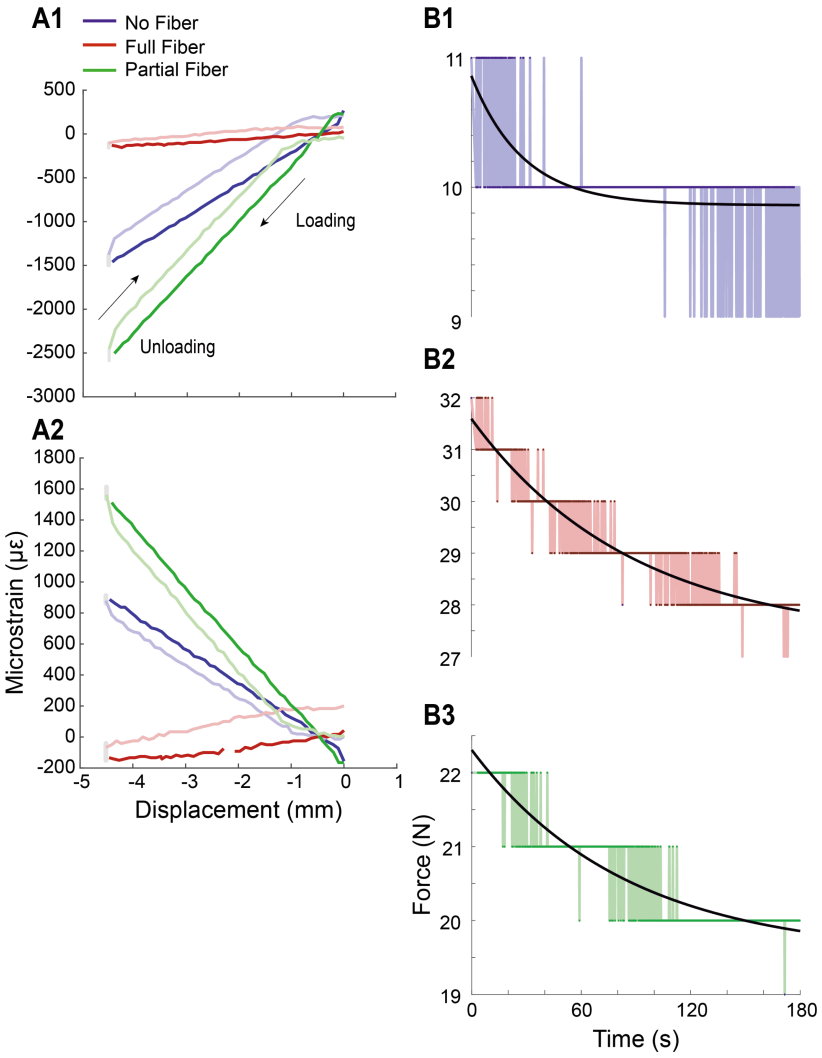

Fig. 3. Strain and force measurements during displacement; **A** microstrain measurements during displacement in each model; low opacity marks increasing displacement, high opacity marks decreasing displacement, grey marks constant displacement; **A1** axial axis; **A2** transverse axis, **B** force measurements during constant displacement test; at a peak displacement of 4.5 mm, the displacement was kept constant for 180 s, allowing the force to vary due to stress relaxation; each force trajectory was fitted using an exponential decay fit; **B1** *no-fiber* model; **B2** *full-fiber* model; **B3** *partial-fiber* model

4 Discussion

To advance the field of distributed sensing in locomoting robotics and to shed light on the effects of material properties on strain sensing, we investigated the effects of Kevlar fiber reinforcement on both displacement and strain sensing in robot limb segments. We utilized a previously published insect-inspired robotic limb and modified it to incorporate Kevlar at different locations. We compared *no-fiber*, *partial-fiber*, and *full-fiber* reinforcement. Fiber reinforcement was placed in the *partial-fiber* model from the distal end to 10 mm from the strain gauge to increase strain measurement while reducing the overall compliance of the limb segment.

Our data clearly showed that the stiffest model was the *full-fiber* model, with the *partial-fiber* model exhibiting about 69% of the *full-fiber* model's stiffness and the *no-fiber* model exhibiting about 34% of the *full-fiber* model's stiffness (Fig. 2B). Despite these differences in stiffness, the strain gauge measurement was highest in the *partial-fiber* model. This strain showed the same trajectory as in the non-fiber model and was, thus, not artificially altered through the partial Kevlar inclusion, unlike the *full-fiber* model, which showed no tension along the transverse axis (Fig. 3A1–2). The *partial-fiber* model, which had no Kevlar fiber in the area of the strain gauge, produced the highest-amplitude strain measurements while maintaining reasonably high rigidity.

The highest SNR was seen in the *no-fiber* model and the lowest SNRs were seen in the *full-fiber* model. The *partial-fiber* models axial SNR was 12.3% lower than the *no-fiber* models axial axis (Table 1). This may be due to error in the application of the strain gauge rosettes, as both the connection to the operational amplifiers and their adherence to the model itself may influence their measurements. Additionally, the constitution of the *partial-fiber* model may amplify environmental noise, such as vibration from the floor. Further study should include a higher number of samples. Another limitation to this study is that the force gauge used to measure the applied force has a resolution of 1 N. In future experiments, a force gauge with more precision should be used.

These findings are not only of interest for robotic manufacturing but also highlight the relevance of the highly complex biological insect cuticle for strain sensing. The cuticle of an insect varies within and between locations in thickness, composition, and layering [12]. Further, recent findings from stick insects have highlighted that mechanical stress relaxation in the cuticle affects the adaptation rates of strain sensors [19]. The present data suggest that the incorporation of more rigid fibers throughout limb segments can affect both hysteresis and strain magnitude, while also indicating that the reinforcement of rigid elements must be nuanced to increase the sensitivity of strain monitoring. Similarly, to the Kevlar fiber-reinforced models used herein, insect cuticle contains anti-parallel alpha-chitin fibers that contribute to overall stiffness through their morphology [11]. As within our *partial-fiber* model, the size of these chitin nanofibrils can vary in locations with high resistance to compression [11, 20], which highlights the benefits of bioinspired, spatially planned fiber reinforcement in robotic limbs. Consequently, to better understand strain sensing in insects, we propose analyzing the material properties of the cuticle surrounding CS and their effects on the purely mechanical aspects of sensor activation.

In conclusion, we analyzed the benefits of Kevlar reinforcement in robotic limbs for walking legs. The data show advantages of partial fiber supplementation for an increase

in rigidness and strain sensing magnitude. Utilizing these findings will further advance the resiliency and robustness of robots.

Funding. IK and NSS were supported by NSF DBI 2015317 as part of the NSF/CIHR/DFG/FRQ/UKRI-MRC Next Generation Networks for Neuroscience Program. IK, NSS, and SNZ were supported by NSF IIS 2113028. GFD was supported by DFG DI 2907/1-1 (Project number 500615768).

Disclosure of Interests. The authors have no competing interests to declare that are relevant to the content of this article.

References

1. Houk, J., Simon, W.: Responses of golgi tendon organs to forces applied to muscle tendon. J. Neurophysiol. **30**, 1466–1481 (1967). https://doi.org/10.1152/jn.1967.30.6.1466
2. Pringle, J.W.S.: Proprioception in Insects: I. A new type of mechanical receptor from the palps of the cockroach. Journal of Experimental Biology **15**, 101–113 (1938)
3. Pringle, J.W.S.: Proprioception in Insects II. The Action of the Campaniform Sensilla on the Legs (1937)
4. Zill, S., Schmitz, J., Büschges, A.: Load sensing and control of posture and locomotion. Arthropod Struct. Dev. **33**, 273–286 (2004). https://doi.org/10.1016/j.asd.2004.05.005
5. Zyhowski, W.P., Zill, S.N., Szczecinski, N.S.: Adaptive load feedback robustly signals force dynamics in robotic model of *Carausius Morosus* stepping. Front. Neurorobot. **17**, 1125171 (2023). https://doi.org/10.3389/fnbot.2023.1125171
6. Dinges, G.F., Zyhowski, W.P., Goldsmith, C.A., Szczecinski, N.S.: Comparison of Trochanteral Strain in Locomotor Model Organisms Using Robotic Legs. Springer (2023)
7. Zyhowski, W.P., Zill, S.N., Szczecinski, N.S.: Load Feedback from a Dynamically Scaled Robotic Model of *Carausius Morosus* Middle Leg. In: Conference on Biomimetic and Biohybrid Systems, pp. 128–139. Springer International Publishing, Cham (2022)
8. Xue, F., et al.: Ultra-Sensitive, Highly Linear, and Hysteresis-Free Strain Sensors Enabled by Gradient Stiffness Sliding Strategy. npj Flex Electron **8**, 1–8 (2024). https://doi.org/10.1038/s41528-024-00301-7
9. Li, P., et al.: Wide range compressed sensing structure based on tension-compression conversion and variable stiffness slope structure. Sci. China Mater. **67**, 871–878 (2024). https://doi.org/10.1007/s40843-023-2748-8
10. Lynch, K.M., Park, F.C.: Modern Robotics: Mechanics, Planning, and Control. Cambridge University Press, Cambridge, UK (2017). ISBN 978-1-107-15630-2
11. Vincent, J.F.V.: Arthropod Cuticle: A Natural Composite Shell System. Compos. A Appl. Sci. Manuf. **33**, 1311–1315 (2002). https://doi.org/10.1016/S1359-835X(02)00167-7
12. Rajabi, H., Jafarpour, M., Darvizeh, A., Dirks, J.-H., Gorb, S.N.: Stiffness distribution in insect cuticle: a continuous or a discontinuous profile? J. R. Soc. Interface **14**, 20170310 (2017). https://doi.org/10.1098/rsif.2017.0310
13. Moran, D.T., Chapman, K.M., Ellis, R.A.: The fine structure of cockroach campaniform sensilla. J. Cell Biol. **48**, 155–173 (1971). https://doi.org/10.1083/jcb.48.1.155
14. Jafarpour, M., Eshghi, S., Darvizeh, A., Gorb, S., Rajabi, H.: Functional significance of graded properties of insect cuticle supported by an evolutionary analysis. J. R. Soc. Interface **17**, 20200378 (2020). https://doi.org/10.1098/rsif.2020.0378

15. Vincent, J.F.V., Wegst, U.G.K.: Design and mechanical properties of insect cuticle. Arthropod Struct. Dev. **33**, 187–199 (2004). https://doi.org/10.1016/j.asd.2004.05.006
16. Kevlar 3D Printing - Specialized Continuous Fiber Available online: https://markforged.com/materials/continuous-fibers/kevlar, Accessed on 5 March 2024
17. Onyx - Composite 3D Printing Material Available online: https://markforged.com/materials/plastics/onyx. Accessed on 22 February 2023
18. Xu, Q., Engquist, B.: A mathematical model for fitting and predicting relaxation modulus and simulating viscoelastic responses. Proceedings of the Royal Society A: Mathematical, Physical and Engineering Sciences **474**, 20170540 (2018). https://doi.org/10.1098/rspa.2017.0540
19. Harris, C.M., Szczecinski, N.S., Büschges, A., Zill, S.N.: Sensory signals of unloading in insects are tuned to distinguish leg slipping from load variations in gait: experimental and modeling studies. J. Neurophysiol. **128**, 790–807 (2022). https://doi.org/10.1152/jn.00285.2022
20. Gardiner, B.G., Khan, M.F.: A new form of insect cuticle. Zool. J. Linn. Soc. **66**, 91–94 (1979). https://doi.org/10.1111/j.1096-3642.1979.tb01903.x